The Thesis Committee for Emily Elizabeth Anderson
Certifies that this is the approved version of the following thesis:

Summer diatom blooms in the eastern North Pacific gyre investigated with a long-endurance autonomous vehicle

APPROVED BY

SUPERVISING COMMITTEE:

Supervisor: _____
Tracy A. Villareal

_____
Cara Wilson

_____
Bryan Black

Summer diatom blooms in the eastern North Pacific gyre investigated with a long-endurance autonomous vehicle

by

Emily Elizabeth Anderson

Thesis

Presented to the Faculty of the Graduate School of

The University of Texas at Austin

in Partial Fulfillment

of the Requirements

for the Degree of

Master of Science in Marine Science

The University of Texas at Austin

December 2017

Dedication

To my wonderful family and friends, thank you for believing in me and supporting me on my journey to improve my understanding of the natural world.

Acknowledgements

I'd like to acknowledge the wonderful support staff at UTSMI in Port Aransas. We couldn't function without you! I'd also like to acknowledge the generous community of Port Aransas and Corpus Christi, TX. The acts and spirit of togetherness after Hurricane Harvey was a balm to my soul during the recovery process. Dr. Tracy Villareal is a very patient advisor, thank you.

Abstract

Summer diatom blooms in the eastern North Pacific gyre investigated with a long-endurance autonomous vehicle

by

Emily Elizabeth Anderson, M.S. MarineSci

The University of Texas at Austin, 2017

Supervisor: Tracy A. Villareal

Summertime phytoplankton blooms regularly develop in the North Pacific subtropical gyre, a region of open ocean that is far removed from any land-derived or Ekman upwelling nutrient sources. Limited direct sampling suggest these blooms are dominated by N_2-fixing diatom-cyanobacteria associations in the genera *Rhizosolenia* and *Hemiaulus*. The nitrogen fixing endosymbionts are hypothesized to be critical to the development of blooms in this nitrogen limited region. However, due to their remote location and unpredictable duration, prolonged *in situ* observations of the environment and biota are rare outside of the major time-series at Station ALOHA. In the summer of 2015, a proof-of–concept mission using the autonomous aquatic vehicle, *Honey Badger* (WaveGlider SV2), collected surface and near-surface (<20m) observations in the NPSG with hydrographic, meteorological, optical, and imaging sensors focusing on the abundance and distribution of these bloom forming symbioses. *Hemiaulus* and *Rhizosolenia* cell abundances were calculated using in-line digital holography for the

entire mission from June-November. While the *Honey Badger* was not able to reach the 30°N subtropical front region where most of the summer diatom blooms have been observed, near-real time navigational control allowed it to transect two bloom regions identified by satellite chlorophyll-a concentrations. The two species did not co-occur in large numbers, rather the blooms were dominated by either *Hemiaulus* or *Rhizosolenia*. The 2-4 August 2015 bloom was comprised of 96% *Hemiaulus* diatoms and second bloom, 15-17 August, was dominated by *Rhizosolenia* diatoms (75%). The holograms also provide valuable insights into the occurrence of aggregated forms of *Hemiaulus* diatoms outside the identified *Hemiaulus* bloom area. The photosynthetic potential index (F_v:F_m) increased during both blooms. In addition, the diel pattern of F_v:F_m (nocturnal maximum; diurnal minimum) was consistent with macronutrient limitation throughout the mission with no evidence of Fe-limitation despite the presence of nitrogen fixing diatom-diazotroph assemblages. By the end of the 5-month mission, *Honey Badger* had covered about 3070 nautical miles (5690 km), taken 9139 holograms, skirted two major tropical storms (Guillermo and Ignacio), and reliably transmitted data to an ERDDAP data server in near real-time.

Table of Contents

List of Tables ix

List of Figures x

Introduction 1

Methods 4

- Location 4
- *Honey Badger* 5
- Holographic imaging 8
- Diatom enumeration 9
- PAM fluorometry (F_v:F_m) 10
- Biovolume analysis 11
- Satellite analysis 12

Results 14

Discussion 29

Conclusion 33

References 34

Vita 41

List of Tables

Table 1. Sensor list and sample frequency.....6

Table 2. *Hemiaulus* aggregate times and locations.....21

List of Figures

Fig 1. *Honey Badger* track. 4

Fig 2. *Honey Badger* diagram and sensor locations. 7

Fig 3. Sample of holograms removed from analysis. 11

Fig 4. gpCTD data....14

Fig 5. Average chl concentration of the study area. 15

Fig 6. Time series comparisons between the Aqua MODIS chl data and the *in situ* data collected by the *Honey Badger*'s sensors. 16

Fig 7. *Hemiaulus* and *Rhizosolenia* cells captured by the Holo. 18

Fig 8. Aqua MODIS chl surface concentration and *Honey Badger*'s position....20

Fig 9. Locations of non-aggregated *Hemiaulus* cells and locations of aggregates.. 22

Fig 10. Scatterplot of aggregated and non-aggregated *Hemiaulus* cells....23

Fig 11. PhytoFlash F_v:F_m diel rhythm sample and iron limitation test.. 24

Fig 12. PhytoFlash F_m diel rhythms before the PhytoFlash failure.. 25

Fig 13. Images from the Downward Facing Camera to compare biofouling. 26

Fig 14. Biovolume calculated from 11-58µm equivalent spherical diameter bins.. 27

Fig 15. C3 fluorometer data from the *Honey Badger*. 28

Introduction

The low-nutrient, low chlorophyll (LNLC) oceanic regimes with chlorophyll-a (chl) concentrations <0.07 mg m^{-3} constitute approximately 60% of the world ocean [1] and are home to a highly adapted phytoplankton community capable of survival at the ambient nanomolar concentrations of inorganic NO_3^- and PO_4^{-2}. One of the important adaptations is nitrogen-fixation (diazotrophy), a process by which abundant dissolved N_2 is converted into ammonium for incorporation into amino acids and proteins [2]. N_2-fixation requires abundant iron resources [3,4] and is reduced in regions that are iron limited [5]. N_2-fixation may also be limited by other nutrients (phosphorous) [3,4,6] or competition by non-diazotrophic phytoplankton [5]. Multiple prokaryote taxa are capable of diazotrophy [7]; photosynthetic taxa include colonial cyanobacteria such as *Trichodesmium* spp. [8,9], free-living coccoid forms including *Crocosphaera watsonii* [10,11], and coccoid or filamentous forms symbiotic with eukaryotes. Of these latter symbioses, there are coccoid forms symbiotic with the prymnesiophyte *Braarudosphaera bigelowii* [12,13], dinoflagellates [14,15] and filamentous or coccoid cyanobacteria occurring as exo- or endosymbionts of diatoms [16,17]. This latter group, diatom-diazotroph associations (DDAs), are dominated by an endosymbiosis between the filamentous cyanobacteria, *Richelia intracellularis*, and members of the diatom genera *Rhizosolenia* and *Hemiaulus*. These symbioses have complex interactions with their hosts [18,19] and the taxonomic distinctness of the symbionts even within a single host genus remains unclear. DDAs play important roles in biogeochemical cycling off the Amazon [20,21] and Mekong Rivers [22] as well as in the central North Pacific gyre [23].

At the Hawai'i Ocean Time-series (HOT), episodic pulses of *Hemiaulus* spp. rapidly sink to depth [24,25] transporting ~20% of the annual carbon flux in a limited window (15 July-15 August) during summer termed the summer export pulse (SEP) [26]. Isotopic signatures of N_2 fixation suggest that their diazotrophic symbiont is present and fueling the biomass flux; the rapid sinking rate indicates aggregation plays a key role in the accelerated transport to depth. The SEP is likely linked to episodic surface blooms of DDAs advecting through the region in the prevailing flow [27–29].

The DDA host genus *Hemiaulus* is a characteristic upper euphotic zone species [30,31] found across the central North Pacific gyre. Near-surface blooms of both *Rhizosolenia* and *Hemiaulus* DDAs [32] extend well north of Hawai'i at abundance up to 10^4 L^{-1} [33–35] and are frequently associated with summer chl blooms observed in satellite ocean color sensors [36,37]. These chl blooms (defined as > 0.15 mg chl m^{-3}) north of 25.5° N cover a much greater range of temperatures and surface area than the blooms at HOT (~22.5° N) and extend at least as far north as 35.5° N [33,38]. While the data suggest that these satellite-observed blooms are probably associated with DDA events, it has remained difficult to sample these more northerly blooms due to the remote location, episodic timing and extensive possible geographic range. The generality of the SEP to these areas is unclear as is the general role of aggregation in *Hemiaulus* spp. biology. *In situ* diver observations suggest aggregation commonly occurs in *Hemiaulus* [34], providing dense units that could quickly sink to depth as the bloom senesces. It is unclear whether *Hemiaulus* aggregation is uniquely localized to the summer export window or is a more generalized feature throughout the year.

In this paper, we present a data set from a long-range autonomous vehicle, an SV2 Wave Glider [39], equipped with a novel array of imaging and physiological sensors. This class of vehicle is capable of multiple-month missions under near-real time control and has successfully transited from Hawai'i to Australia while returning oceanographic data [40]. In this paper, we present data gathered during a 5-month mission in 2015 which sampled two diatom blooms. The mission objectives were to determine if an off-the-shelf holographic imaging system could quantify diatom events, relate the observed imagery and PhytoFlash data to satellite observed chl blooms, and examine the data for evidence of aggregation. We were able to derive community biovolume estimates and describe the potential effects of biofouling on the optical quantification.

Methods

LOCATION

The mission area for the *Honey Badger* was the eastern North Pacific subtropical gyre (NPSG) spanning from 19-30°N and -144 to -157°W in the open waters northeast of the Hawaiian Islands (Fig 1) where chl blooms regularly occur between July and October [37]. Waypoints were chosen after consulting Aqua-MODIS 8-day composite chl concentration satellite images from ERDDAP (https://coastwatch.pfeg.noaa.gov/erddap/griddap/erdMBchla8day.html) to direct *Honey Badger* into regions where blooms were observed or predicted. After a preliminary deployment in the Liquid Robotics test area off Kawaihae, Hawai'i, the *Honey Badger* headed north on 1 June 2015. It was recovered on 3 November 2015 and returned to the test facility for evaluation and data download.

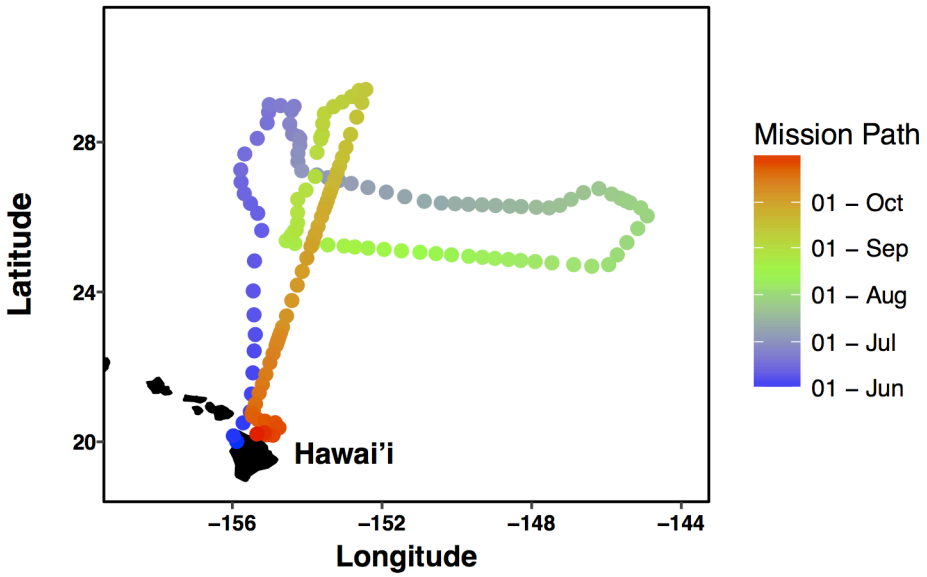

Fig 1. *Honey Badger* track. The average daily coordinates of the *Honey Badger* during the 153-day mission from 1 June- 3 November 2015.

HONEY BADGER

The Liquid Robotics, Inc. (LRI; Sunnyvale, CA) Wave Glider® SV2 is an autonomous surface vehicle capable of extended operations offshore. The Wave Glider® we used was designated *Honey Badger*. It has a surface float (2.1 m X 0.6 m) connected by a 7 m umbilical to a subsurface glider (0.4 m X 1.9 m) with articulating wings (1.1 m wide) that use vertical motion from waves to provide forward motion. Within the surface float, equipment bays provide space for computers, communications equipment and battery arrays powered by solar panels. Details of the buoyancy, communication, speed and power supplies are discussed in Hine [41]. Iridium satellite communication with the Wave Glider was in near-real time and provided a near immediate ability to course correct and respond to environmental conditions. LRI-provided sensors were augmented with a novel configuration of an active fluorescence sensor and a holographic imaging sensor.

The *Honey Badger* was equipped with sensors on the float, the sub-body, and a towed body (Table 1) (Fig 2). The float contained 2 Turner Designs C3 fluorometers (Sunnyvale, CA) rimmed with anti-fouling copper, a Seabird Electronics gpCTD (Bellevue, WA) for water temperature and salinity with an inline antifouling tablet, a Canon G10 camera (Canon, USA Inc, Melville, NY) looking down through the float, a Datawell MOSE weather sensor (Datawell BV, Haarlem, The Netherlands), Airmar WX and WS weather sensors+light bar (Airmar Technology Corporation, Milford, NH), an AIS (automatic identification system) transponder and a radar reflector. The sub-body located 7m below the float had an externally mounted Turner Designs PhytoFlash (Sunnyvale, CA) utilizing the data and power connections through the umbilical. A Sequoia Scientific, Inc. (Bellevue, WA) Laser *In Situ* Scattering and Transmissometry Holographic System (LISST-Holo, Holo) holographic imaging sensor was deployed in a towed

body behind the *Honey Badger* on a 10 m tether which imaged the water between 6.3-15.5m. The Holo was powered using the power from the umbilical with the data stored in the Holo's onboard internal memory module. Bandwidth limitations did not permit transmission to shore via Iridium satellite. The Holo sample chamber was painted with antifouling paint with copper tape on other surfaces to minimize fouling. Sensors were integrated into the onboard processing and communications equipment by LRI with the exception of the PhytoFlash. Software integration for the PhytoFlash and initial tow body design was provided by the Geophysical Engineering Research Group at Texas A&M University.

Sensor (location)	**Variables (units)**	**Interval**	**Available in Near Real Time?**
Sea-Bird Scientific's gpCTD (1)	Water Temperature (°C), Salinity (PSU), Density (dBar)	48 hr^{-1}	Yes
Turner Designs' C3™ Submersible Fluorometer with Antifouling Coating (1)	Colored Dissolved Organic Mater (CDOM) (RFU), Chlorophyll-a (RFU), and Phycoerythrin Fluorescence (RFU)	6 hr^{-1}	Yes
Turner Designs' C3™ Submersible Fluorometer without Antifouling Coating (1)	Colored Dissolved Organic Mater (CDOM) (RFU), Chlorophyll-a (RFU), and Phycoerythrin Fluorescence (RFU)	6 hr^{-1}	Yes
AirMar Technology's WX Series Ultrasonic WeatherStation® (1)	Air Temperature (°C), Pressure (mBar), Average Wind Speed (knots) and Direction (degrees true)	6 hr^{-1}	Yes
Datawell BV's MOSE (1)	Significant wave height (m) and Direction (degrees true)	2 hr^{-1}	Yes
Cannon G10 Camera (1)	Downward facing camera for imaging the sub-body	6 hr^{-1}	No
Turner Designs' PhytoFlash (2)	F_o, F_m, F_v, Yield (F_v:F_m)	6 hr^{-1}	Yes
Sequoia Scientific LISST-Holo (3)	Holographic microscopic images of the water	1 burst of 15 images every 6 hr	No

Table 1. Sensor list and sample frequency. List of the instruments onboard the *Honey Badger* with their locations on the wave glider (Fig 2) and their programmed sample frequency.

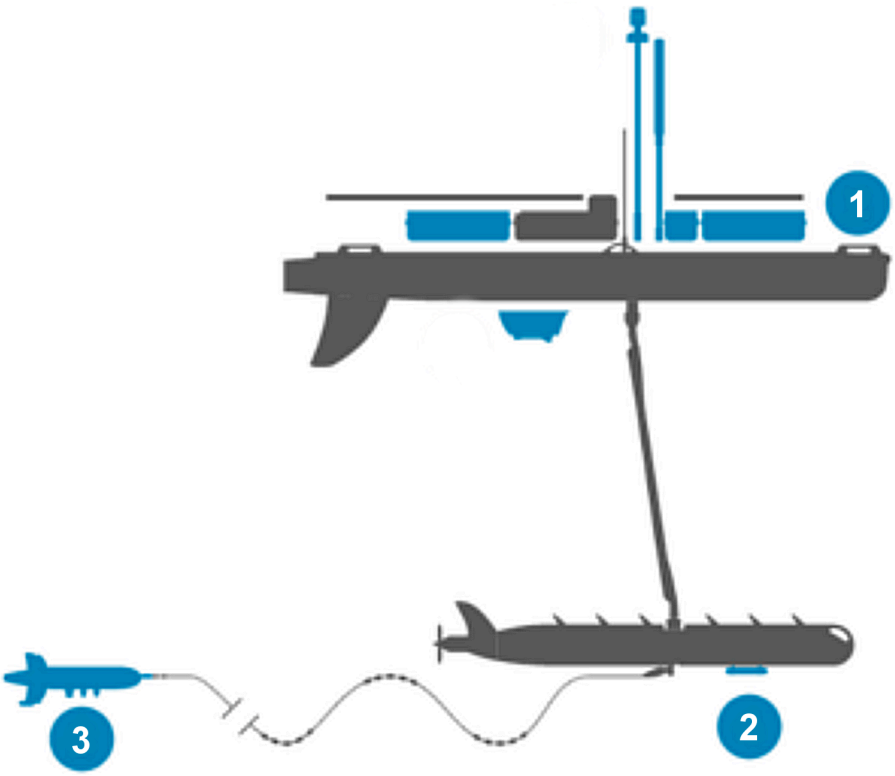

Fig 2. *Honey Badger* diagram and sensor locations. Float body = 1. Sub-body = 2. Tow body = 3. Figure after Liquid Robotics, Inc. [42].

The Turner C3s are multiple head sensors and were equipped with filters for chl, phycoerythrin and CDOM (colored dissolved organic material). Due to the challenges of calibration over a long-term deployment, values are reported in uncorrected fluorescence units. The C3 sensors were deployed on either side of the centerline with a port and starboard sensor. The port C3 sensor and optical port for the look-down camera were coated with a ~30 µm layer of ClearSignal antifouling compound (Severn Marine Technologies, Annapolis, MD) in spring, 2014. Due to technical difficulties, the mission was delayed a year with unknown effects on the viability of the coating. The look-down camera began recording on 1 July 2015, approximately a month after the mission initiation, and imaged vertically below the float for examining the

umbilical and glider as needed but also captured images of fish and biofouling over the course of the mission.

Power consumption and available solar charging dictated sampling frequency and varied with the sensors: gpCTD (10 min), G10 camera (0800, 1200, 1600 local), MOSE (30 min), Airmar (30 min), PhytoFlash (10 min), Holo (every 6 hours; 15 images at 30 sec intervals). The vehicle reported location and condition telemetry every 30 seconds. The PhytoFlash sampled at 10 minute intervals but was accelerated to 1 minute intervals from 27-28 July to test the system's resiliency to increased sampling rates. The port C3 sensor was on a fixed 10 min sampling interval with 10 samples averaged to generate a single value. The starboard sensor was reprogrammable via remote communications and was varied in sampling timing and averaging at various points in the mission. Changes from multi-point averaging to single point reporting resulted in the systematic and predictable baseline shifts. The reasons for these changes are unknown.

HOLOGRAPHIC IMAGING

The Holo allowed us to image and enumerate diatoms that passed through the sampling chamber. The Holo records particle images by capturing refraction patterns from collimated lasers beamed through the sampling field which produces a hologram of the sample field [43,44]. The hologram produced consists of a greyscale representation of the beam scattering. Software provided by Sequoia Scientific Inc. (https://www.sequoiasci.com/product/lisst-holo/) was used to reconstruct the holograms. Holo_Batch (v3.1) was used to reconstruct multiple holograms and export particle data; Holo_Detail (v3.1) was used to scan through each hologram for in-focus particles to identify specific cells, organisms, or artifacts. The Holo took 15 holographic images every 6 hours for the duration of the 5-month mission. Sampling rate for the Holo was set prior

to launch based on worst case power consumption calculations and could not be modified once underway.

The large file size (~2 MB) of each raw Holo hologram precluded satellite transmission and were only available for analysis after the *Honey Badger*'s recovery in November 2015. Upon recovery of the drive, 9336 holographic images were analyzed with the Holo_Batch and Holo_Detail at the University of Texas at Austin's Marine Science Institute. Comparison of Holo_Batch processing and individual Holo_Detail processing of the same images indicated progressive loss of recognizable diatoms over the mission. In addition, the lightly silicified *Hemiaulus* and *Rhizosolenia* of interest often did not process well in the Holo_Batch mode Therefore, *Hemiaulus* and *Rhizosolenia* cells were quantified using the Holo_Detail software on every hologram with recognizable diffraction patterns indicating particles were present. While using the Holo_Detail to enumerate diatoms was more time-intensive than using the montages of in-focus particles produced by the Holo_Batch, it was necessary as the montages often failed to show *Hemiaulus* or *Rhizosolenia* cells in-focus or at all.

DIATOM ENUMERATION

The 15-image bursts taken every 6 hours were combined to form one record yielding 4 records (bursts) d^{-1}. The Holo sampling volume was 1.86 ml per image with the 15-image burst sampling a total of 27.9 ml. Initial dye studies prior to launch indicated the 30 second timing between images was sufficient for full chamber replacement.

The Holo's sampling capability allows counting cells with a minimum concentration of 36 cells L^{-1}. *Hemiaulus* cells occurred as both individual chains and aggregations of various size. Chains described 3 or more *Hemiaulus* cells which formed a curve with clear ends which did not

cross itself or others more than once. Aggregates were defined as *Hemiaulus* cells in a chain or multiple chains with multiple ends or no discernable ends which crossed itself, other chains, or other particles multiple times. Individual *Hemiaulus* cells were hard to differentiate from other small cells so these cells were identified only when they were in a chain or aggregate form.

PAM FLUOROMETRY (F_V:F_M)

Pulse Amplitude Modulation fluorometry by the Turner PhytoFlash was used to evaluate phytoplankton physiological health. In addition, iron stress was evaluated using the variable fluorescence criteria of Behrenfeld and Milligan [45]. Two unique aspects of the PhytoFlash required data manipulation in order to apply the Behrenfeld and Milligan [45] criteria. First, the PhytoFlash was operating at the limits of its sensitivity so time averaging was required to obtain a stable signal since power management requirements did not permit sustained sampling at the high frequencies used in Behrenfeld and Milligan [45]. Second, to avoid the crepuscular excursions in the F_v:F_m signal as seen by Behrenfeld and Milligan [45], the period from 0800-1359 UTC was used to calculate a nighttime average (36 data points) and the period from 1800-0259 UTC (54 data points) was used to calculate a daytime average (PhytoFlash sample frequency=6 samples hr^{-1}). In a macronutrient limited environment with sufficient iron, the nocturnal F_v:F_m is greater than the diurnal F_v:F_m. In an iron limited environment, the reverse is true. The PhytoFlash frequently shutdown and missed samples. To ensure a thorough sampling of daytime and nighttime periods, only periods with 75% or more of the expected number of samples were included in the iron-limitation analysis. Further, to ensure a quantitative comparison between nighttime and daytime values, both periods for a date were required to meet

the above standard. This resulted in the removal of 33 of 94 days of data due to PhytoFlash shutdowns to compare the nocturnal and diurnal F_v:F_m values.

BIOVOLUME ANALYSIS

The Holo_Batch processed all holograms generated during the mission and returned calculated biovolume for all detected particles >10 μm after calculating their equivalent spherical diameter. The biovolume was automatically separated into bins based on equivalent spherical diameter from 2.5μm – 9847 μm (50 bins with the upper size limit of each bin being 1.18 times the lower limit). The diatoms of interest in this study have an equivalent spherical diameter between 13-60 μm so a subset of bins (13.092-58.1μm) were chosen to focus the analysis. Holograms with schlieren (optical anomalies in transparent mediums), microbubbles or blank images (Fig 3) were removed from our analyses.

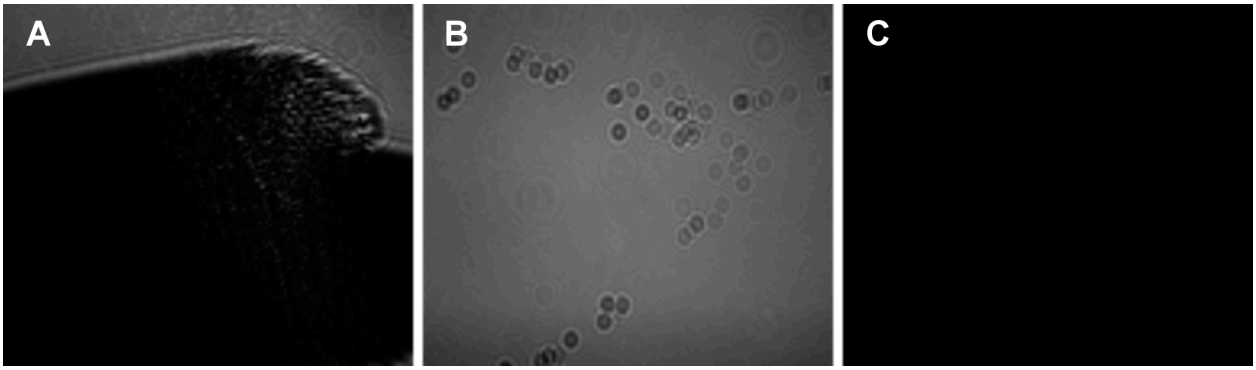

Fig 3. Sample of holograms removed from analysis. Holograms with these characteristics had errors that prevented accurate biological particle volume calculations. A) schlieren, B) microbubbles, C) blank/malfunction hologram.

Biofouling of optical surfaces is a problem for long-term deployments. The manufacturer's recommendation was to average the biovolume over large groups of images to generate a constant signal that represented a consistent particle presence. We averaged groups of 510 holograms representing an 8.5-day window for a total of 14 background signatures. This

signature was subtracted from each hologram in the specified window to generate a biofouling-corrected biovolume. The results were plotted in a time series for comparison with the other observations made by the instruments on the *Honey Badger* and the satellite data.

SATELLITE ANALYSIS

The Aqua MODIS satellite's 8-day composite chl data (https://coastwatch.pfeg.noaa.gov/erddap/griddap/erdMBchla8day.html) were used in conjunction with *Honey Badger*'s positon to compare on-board sensor data with the satellite observed chl data. The daily data from the satellite were downloaded as a .csv file and transformed in ArcMap [46] to produce daily rasters of the chl landscape of the NPSG. The rasters and *Honey Badger*'s location were exported as individual maps and joined chronologically to produce an animation showing the development of the blooms in the NPSG during the 2015 bloom season (June-November). Satellite-derived chl was compared to *Honey Badger* biovolume, cell counts and fluorescence data. The compared data was plotted using RStudio [47].

The 8-day composite images and data from the Aqua MODIS satellite (https://coastwatch.pfeg.noaa.gov/erddap/griddap/erdMBchla8day.html) were mapped with ArcMap and graphed with RStudio to correlate the satellite measurements and the *in situ* data provided by the *Honey Badger*. The satellite data were also used to calculate the average chl concentration for the study area for each day to show how it varied over time.

The raw data from the C3s, gpCTD, AIS, MOSE, PhytoFlash, and weather station are archived at both the NOAA ERDDAP site (http://coastwatch.pfeg.noaa.gov/erddap/search/index.html?page=1&itemsPerPage=1000&searchFor=liquidr) and BCO-DMO under project 505589 (http://www.bco-dmo.org/project/505589).

The BCO-DMO site also contains the raw holograms, the biovolume data, and the *Hemiaulus* and *Rhizosolenia* abundance data.

Results

Honey Badger collected 5 months of salinity, surface water temperature, diatom abundance, photosynthetic activity, and biovolume data from the NPSG. The grey line in Fig 4 shows the 9-point running average used to smooth the raw temperature and salinity measurements. Nine-point and daily smoothing were used to remove changes due to rain events or sensor errors. The daily averaged water salinity and temperature data (Fig 4-black line) ranged from 22.8 to 27.8°C, and 34.6 to 35.6 salinity and indicate that the *Honey Badger* stayed south of the sub-tropical front which is characterized by a salinity of ~34.5 [48].

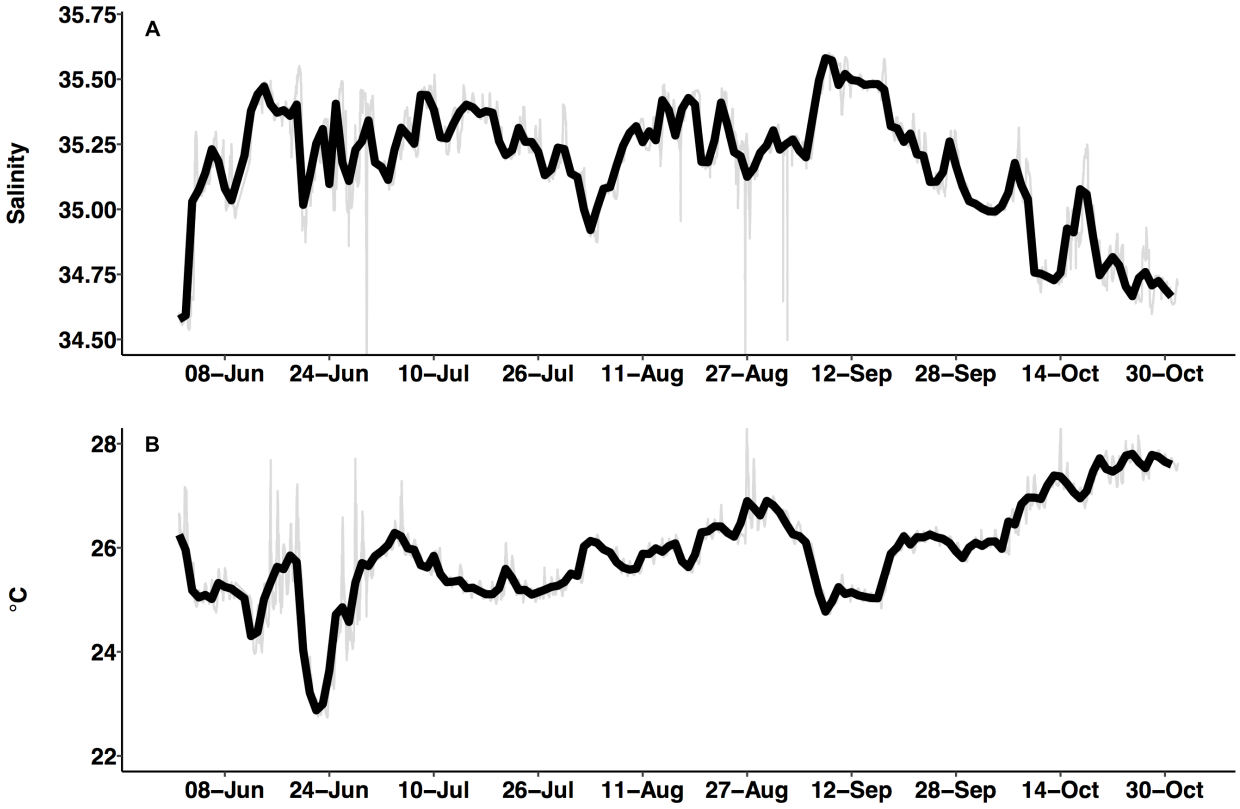

Fig 4. gpCTD data. Time series of the hydrographic properties from the *Honey Badger*'s gpCTD sensor. A) Salinity (PSU). B) Temperature (°C).

The chl animation from the Aqua MODIS data (https://youtu.be/xYE39ua_NTc) shows a uniformly low chl concentration throughout the study area in June 2015 (Fig 5). The background chl started to increase ~1 July 2015 concurrent with a chl variability increase when patches developed with elevated chl. Within the region, there were multiple blooms where the chl exceeded 0.20 mg m^{-3}. The highest chl concentrations which *Honey Badger* sampled were on 2 August 2015 and 17 October 2015 both with chl concentrations of 0.12 mg m^{-3} (Fig 6).

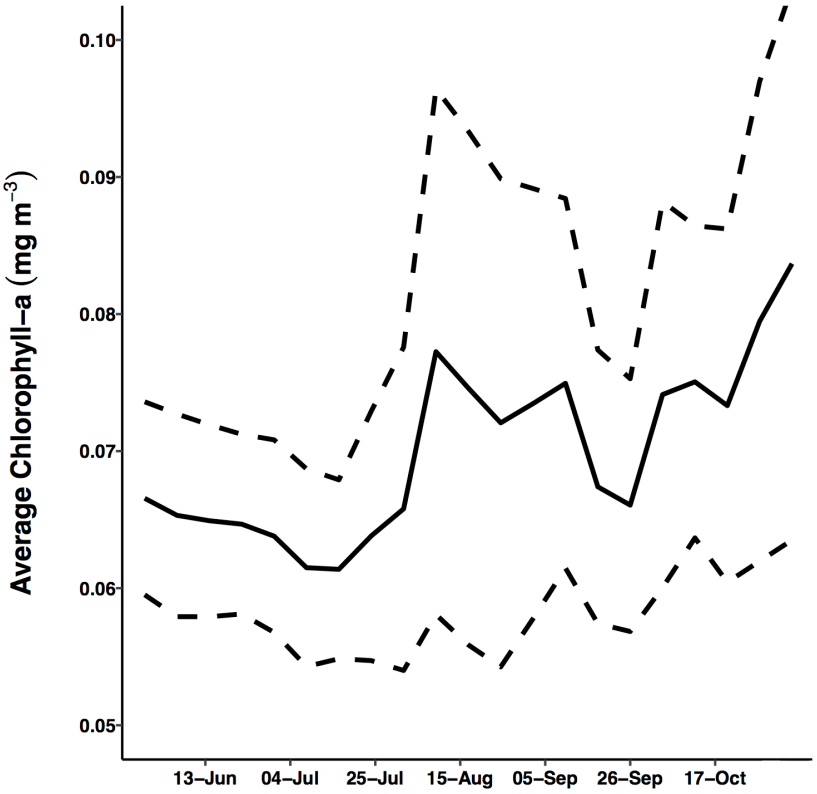

Fig 5. Average chl concentration of the study area. The average of the data points from Aqua MODIS's 8-day composite data within the study area. Solid line = average chl concentration for the study area. Dashed lines = average chl concentration ± 1 standard deviation.

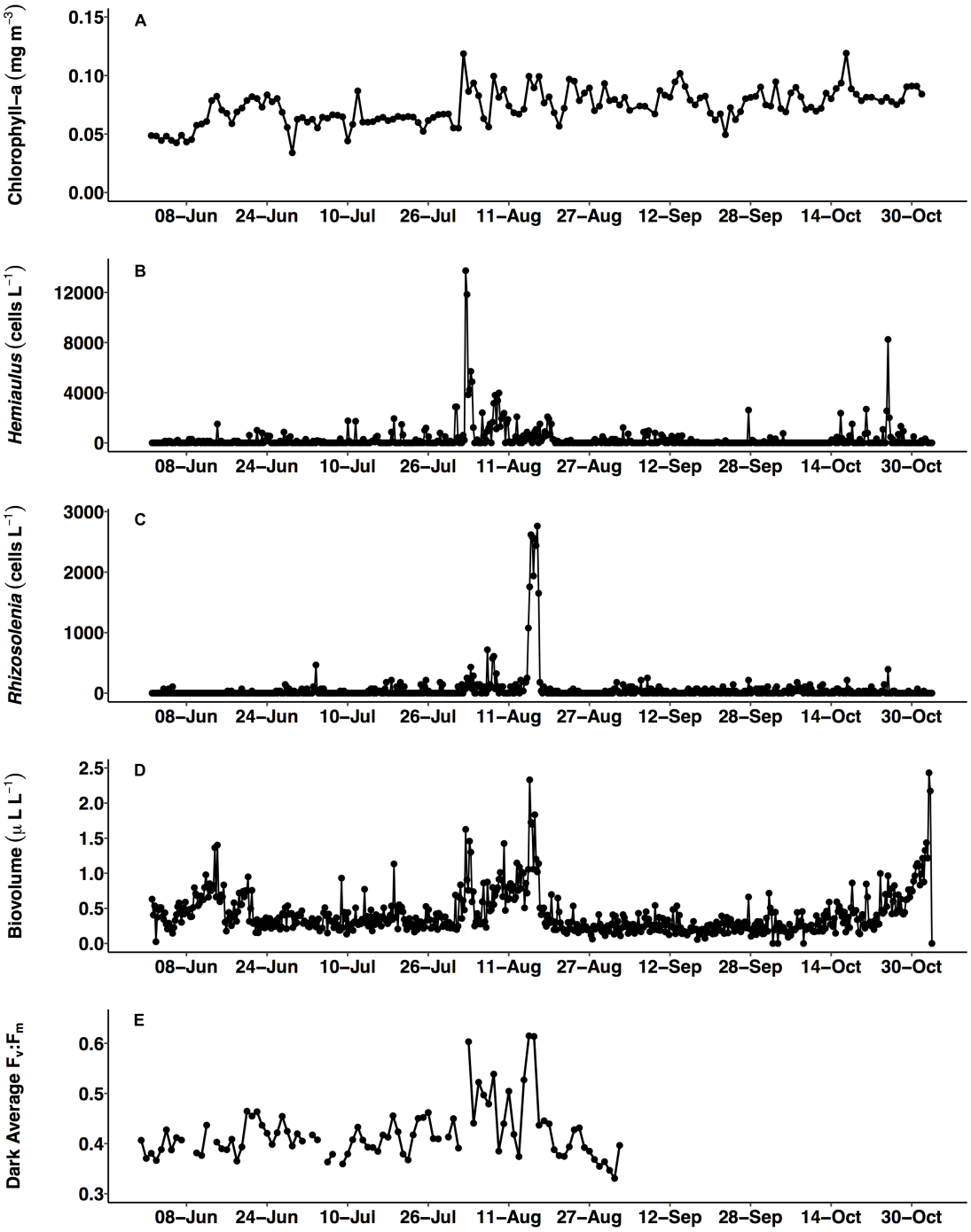

Fig 6. Time series comparisons between the Aqua MODIS chl data and the *in situ* data collected by the *Honey Badger*'s sensors. A) 8-day composite data from Aqua MODIS showing surface chl concentrations (mg m^{-3}) near *Honey Badger*'s location. B and C) *Hemiaulus* and *Rhizosolenia* abundance as counted in the holographic images captured by the Holo and scaled to cells L^{-1}. D) Biovolume from 11-58 μm bins E) Average F_v:F_m between 0800-1359 UTC.

Hemiaulus and *Rhizosolenia* cells were readily identifiable in the processed holograms (Fig 7). *Hemiaulus* maximum abundance was 1.4 x 10^4 cells L^{-1} on 2 August 2015 and the *Rhizosolenia* maximum abundance was 2.8 x 10^3 cells L^{-1} on 16 August 2015 (Fig 6B and 6C). There was a high degree of patchiness in the diatom abundance. Mean *Hemiaulus* abundance was 303 cells L^{-1} (s.d. = 1.0 x 10^3 cells L^{-1}, n = 610) and mean *Rhizosolenia* abundance was 63 cells L^{-1} (s.d. = 2.7 x 10^2 cells L^{-1}, n = 610) over all the samples. However, of the 610 samples, only 208 contained *Hemiaulus* cells and 207 contained *Rhizosolenia* cells. When present, the average *Hemiaulus* abundance was 8.9 x 10^2 L^{-1} (s.d. = 1.6 x 10^3 cells L^{-1}, n = 208). Of the samples containing *Rhizosolenia* cells, the average abundance was 1.8 x 10^2 cells L^{-1} (s.d. = 4.5 x 10^2 cells L^{-1}, n = 207).

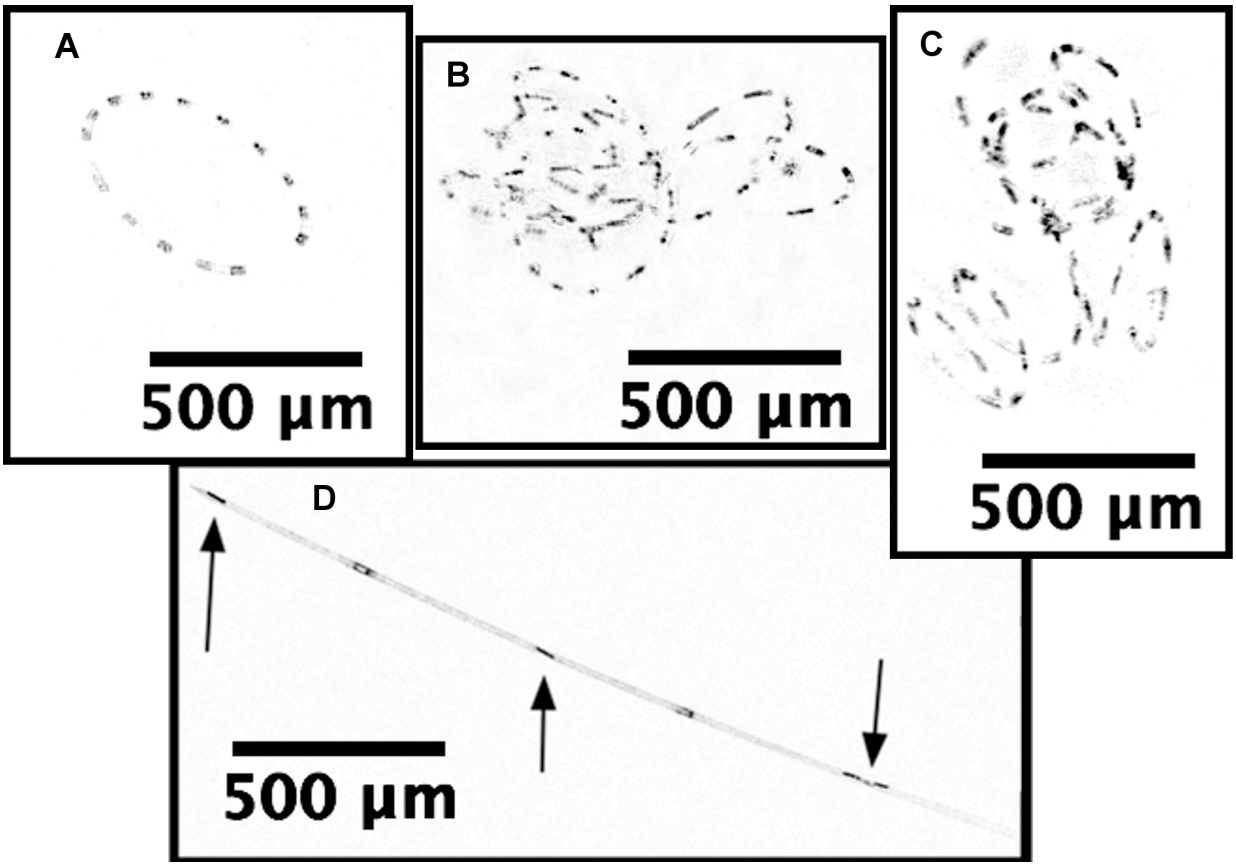

Fig 7. *Hemiaulus* and *Rhizosolenia* cells captured by the Holo. Images produced by the Holo_Batch's reconstructed slices and ImageJ software [49]. Depth refers to depth within hologram image. A) *Hemiaulus* chain. Hologram number: 3905, depth: 7.5mm, timestamp: 8/2/2015 10:18:05 AM (UTC). B and C) *Hemiaulus* aggregates. B) hologram number: 8323, depth: 38mm, timestamp: 10/15/2015 9:19:32 PM (UTC). C) hologram number: 4233, depth: 9.2mm, timestamp: 8/8/2015 12:30:54 AM (UTC). D) *Rhizosolenia* chain. Arrows indicate *Richelia intracellularis* endosymbionts. Hologram number: 7237, depth: 9.0mm, timestamp: 9/27/2015 2:21:15 PM. Brightness and contrast enhanced for publication.

The two blooms sampled, a *Hemiaulus* bloom on 2-4 August 2015 and a *Rhizosolenia* bloom on 15-17 August 2015, were identified by the Holo dataset as periods when the *Hemiaulus* or *Rhizosolenia* abundances were significantly higher than the background values. The *Hemiaulus* bloom was dominated by *Hemiaulus* diatoms (96%) while the *Rhizosolenia* bloom was dominated by *Rhizosolenia* diatoms (75%). The two blooms were separated in space

and in time (Fig 8). The *Honey Badger* sampled the *Hemiaulus* bloom from 2-4 August 2015 when the chl signature was still developing according to the satellite data. The Aqua MODIS animation (https://youtu.be/xYE39ua_NTc) shows the chl signature associated with the *Hemiaulus* bloom continuing to develop after the *Honey Badger* left the area. The *Rhizosolenia* bloom sampled by the *Honey Badger* from 15-17 August 2015 did not have a well-defined bloom chl signal.

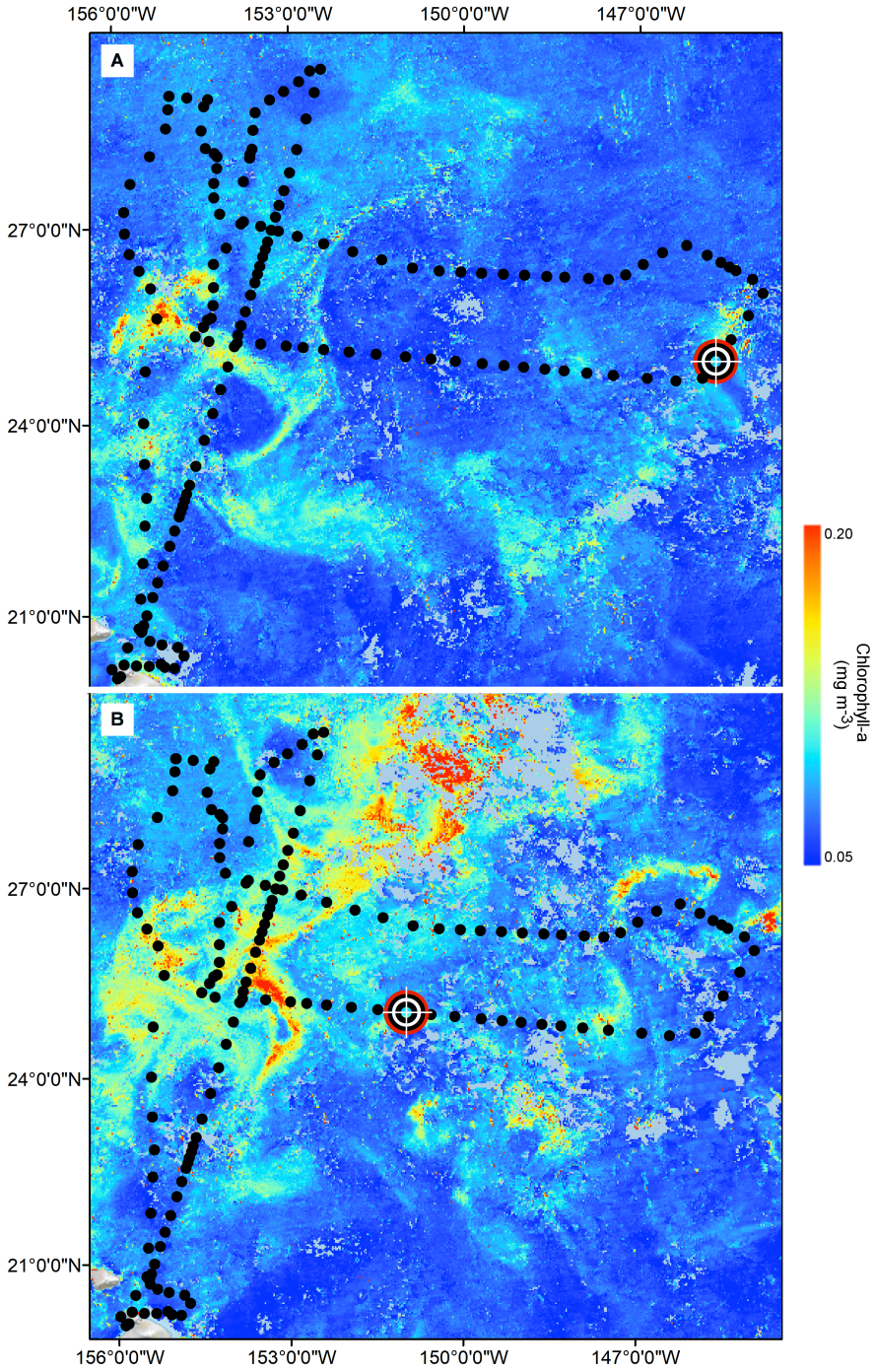

Fig 8. Aqua MODIS chl surface concentration and *Honey Badger*'s position. Black dot= mission track position, red-white-black target = *Honey Badger*'s position on day of satellite image. A) 3 August 2015. Surface chl concentration for the *Hemiaulus* bloom detected at *Honey Badger*'s position. B) 16 August 2015. Surface chl concentration for the *Rhizosolenia* bloom detected at *Honey Badger*'s position.

The Holo captured 33 *Hemiaulus* aggregates at 24 locations (Table 2 and Fig 9). Aggregates were observed between 27 June 2015 and 25 October 2015 outside the time window of the SEP (green shading in Fig 9), They also were not limited to regions where non-aggregated *Hemiaulus* cells were abundant (Fig 10). Within the holograms containing *Hemiaulus* aggregates, the average number of identifiable aggregated cells was 47 (s.d. = 42, n = 31) with a minimum of 5 and a maximum of 220. Due to the complex 3D structures of some of the aggregates, it is possible that not all of the cells were counted in the aggregates. The cell counts for aggregates could be underrepresented.

Aggregate events outside the SEP				**Aggregate Events within the SEP**			
Timestamp (UTC)	**n**	**Latitude**	**Longitude**	**Timestamp (UTC)**	**n**	**Latitude**	**Longitude**
6/27/15 8:07	1	28.417	-154.454	7/20/15 17:16	2	26.252	-147.684
7/10/15 1:06	1	26.685	-151.958	7/31/15 15:33	1	25.887	-145.012
8/17/15 4:01	1	25.097	-151.447	8/2/15 10:15	3	25.240	-145.518
8/18/15 16:37	1	25.153	-152.149	8/3/15 4:34	1	24.996	-145.709
8/19/15 10:55	1	25.183	-152.515	8/3/15 10:40	3	24.927	-145.763
9/2/15 16:29	1	27.444	-153.735	8/5/15 17:34	2	24.710	-146.648
9/27/15 14:14	1	26.120	-153.579	8/8/15 0:27	1	24.805	-147.825
10/15/15 21:22	1	21.888	-155.075	8/8/15 6:33	2	24.814	-147.932
10/20/15 23:22	2	20.812	-155.455	8/9/15 19:08	1	24.860	-148.503
10/21/15 5:28	1	20.771	-155.469	8/10/15 1:13	1	24.865	-148.570
10/25/15 0:58	2	20.545	-155.179	8/13/15 20:43	1	24.982	-150.015
10/25/15 7:04	1	20.562	-155.107				
10/25/15 13:10	1	20.537	-155.034				

Table 2. *Hemiaulus* aggregate times and locations. The *Hemiaulus* aggregate events outside (left) and within (right) the 15 July – 15 August SEP [26]. N = number of aggregates in each record.

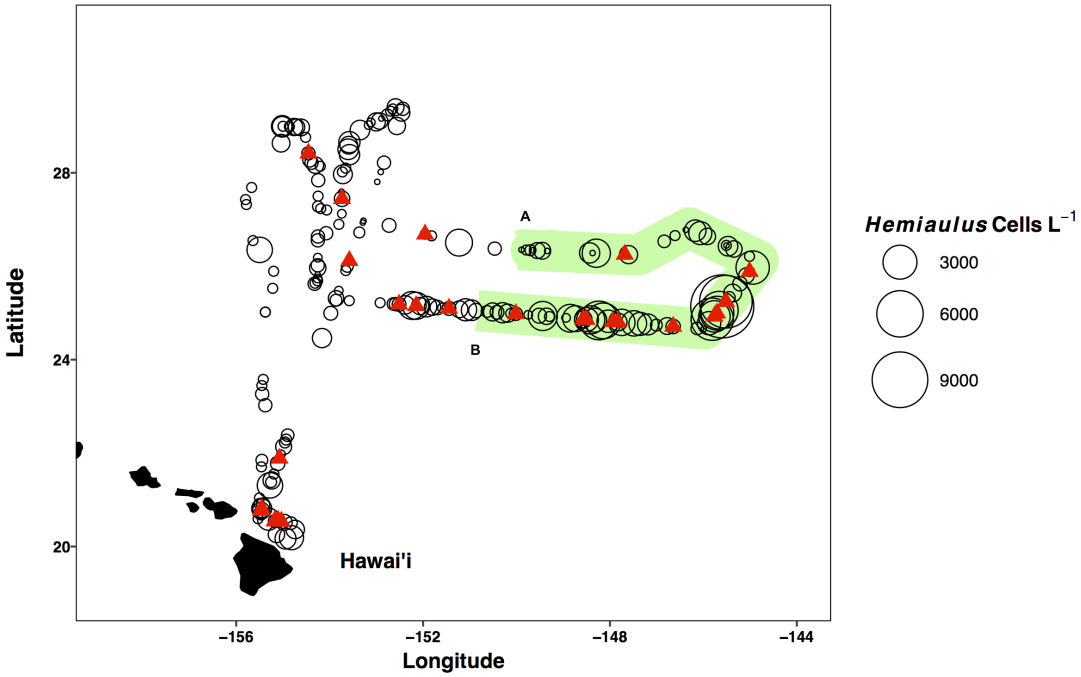

Fig 9. Locations of non-aggregated *Hemiaulus* cells and locations of aggregates. Red triangle = aggregate. Circles = non-aggregated *Hemiaulus* cells L^{-1}, size is indicative of abundance. The green area indicates where *Honey Badger* sampled during the SEP time window (15 July– 15 August).

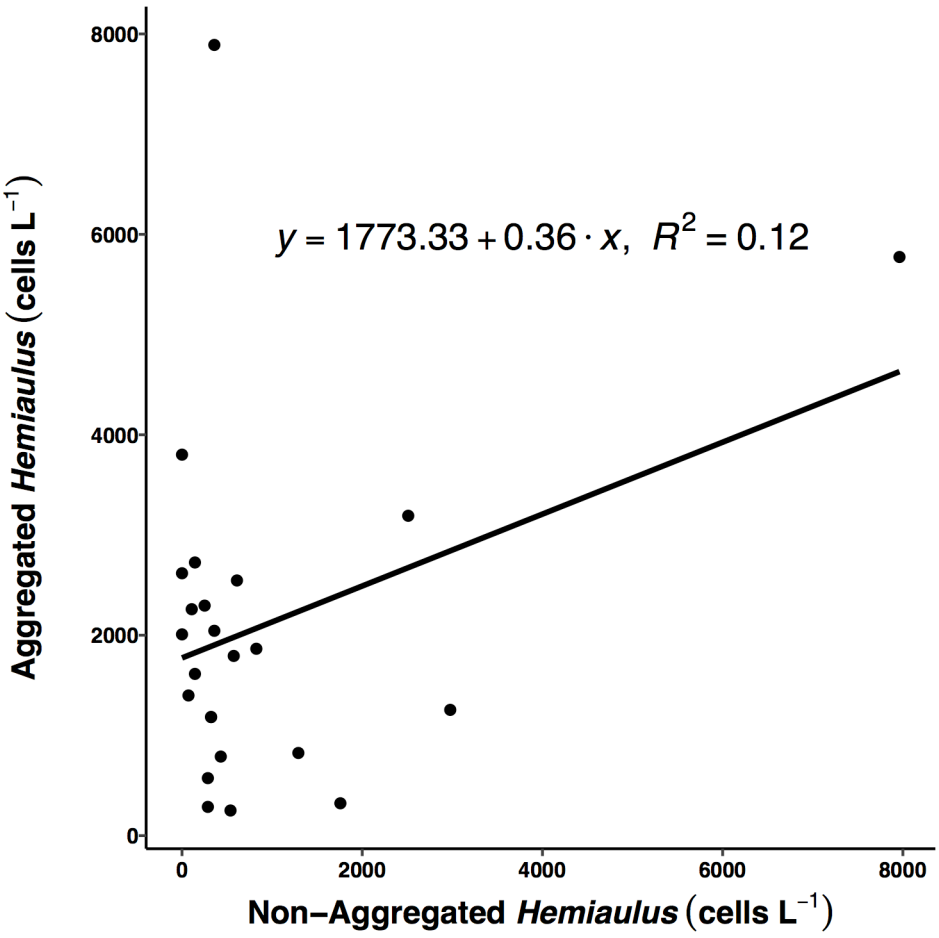

Fig 10. Scatterplot of aggregated and non-aggregated *Hemiaulus* cells. Aggregate observations are poorly correlated with no significance (p = 0.5) to non-aggregated *Hemiaulus* concentrations.

The F_v:F_m values were greatest in the dark period and lower during the daytime (Fig 11A). From visual inspection of the entire mission dataset, there was no reversal of the diel rhythm. The diurnal:nocturnal F_v:F_m ratio remained positive indicative of a macro-nutrient limited environment (Fig 11B) [50]. The negative value on 1 September 2015 was the result of the PhytoFlash failing as the F_o and F_m values start behaving abnormally around 1 September 2015 04:00 UTC (Fig 12). These were the last dates with uncompromised data before the PhytoFlash shutdown on 9 September 2015.

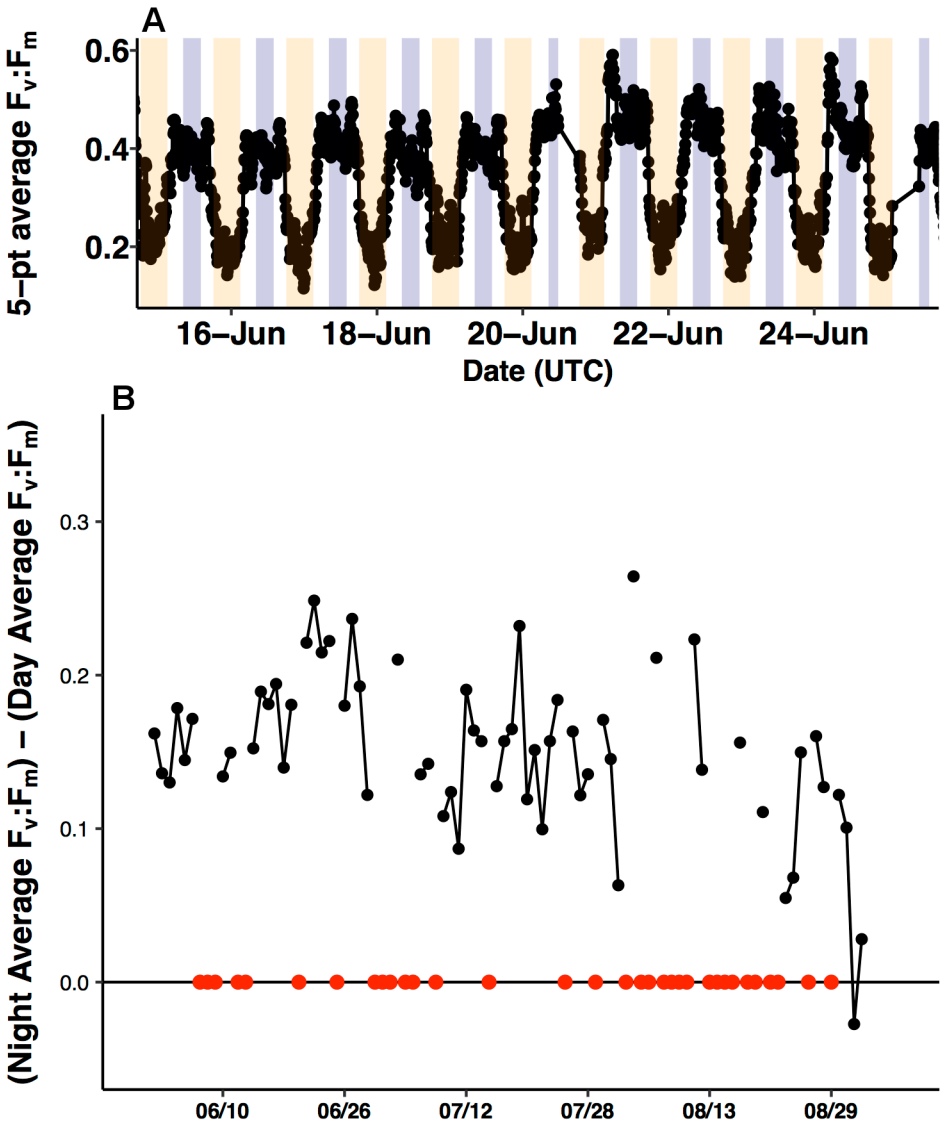

Fig 11. PhytoFlash F_v:F_m diel rhythm sample and iron limitation test. A) Sample of the typical diel rhythm observed in the PhytoFlash's F_v:F_m measurements. The signal is downregulated during the daytime and unaffected during the dark period. Dark bars = 08:00-13:59 UTC (nocturnal period). Light bars = 18:00-02:59 UTC (diurnal period). B) Time-series of the dark-averaged F_v:F_m minus the light-averaged F_v:F_m. Red points indicate where the sample number did not meet the threshold for calculation (see Methods).

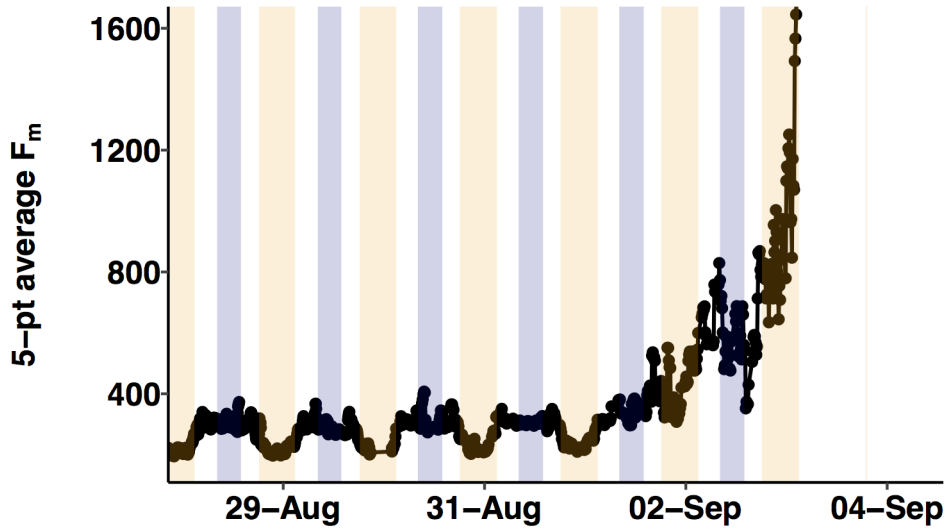

Fig 12. PhytoFlash F_m diel rhythms before the PhytoFlash failure. F_m values showing the normal (nocturnal maxima; diurnal minima) diel rhythms of the mission up to 1 September 2015. Dark bars = 08:00-13:59 UTC (nocturnal period). Light bars = 18:00-02:59 UTC (diurnal period).

The biovolume increased during the two blooms (Fig 6D). The average biovolume for the mission was 0.42 µL L^{-1} (s.d. 0.30, n = 610). During the *Hemiaulus* bloom (2-4 August 2015), the average biovolume was 0.77 µL L^{-1} (s.d. = 0.47, n = 12) with a maximum biovolume of 1.63 µL L^{-1} recorded on 8/2/2015 10:15:33 UTC. The average biovolume during the *Rhizosolenia* bloom (15-17 August 2015) was 1.16 µL L^{-1} (s.d. = 0.63, n = 12) and the maximum biovolume of 2.33 µL L^{-1} was recorded on 8/15/2015 3:14:02 UTC. As the diatom abundance increased, the biovolume increased as well (r^2=0.1175). However, there were some instances where the biovolume increased without a corresponding increase in diatom abundances as seen around 15 June 2015 and after 20 October 2015. There was also an increase in biovolume after 20 October 2015. At this time, the *Honey Badger* was entering the waters close to the Hawaiian Islands but the diatom numbers did not appear to be the drivers of the increase and the holograms did not

show any recognizable particles for enumeration. Biofouling was obvious later in the mission, particularly on the Downward-facing camera images (Fig 13) and in the biovolume calculations by the Holo_Batch (Fig 6D). In Fig 14, the percent of biovolume removed after calculating the background biovolume approaches 100% suggesting that biofouling on the optics had become too great for correction.

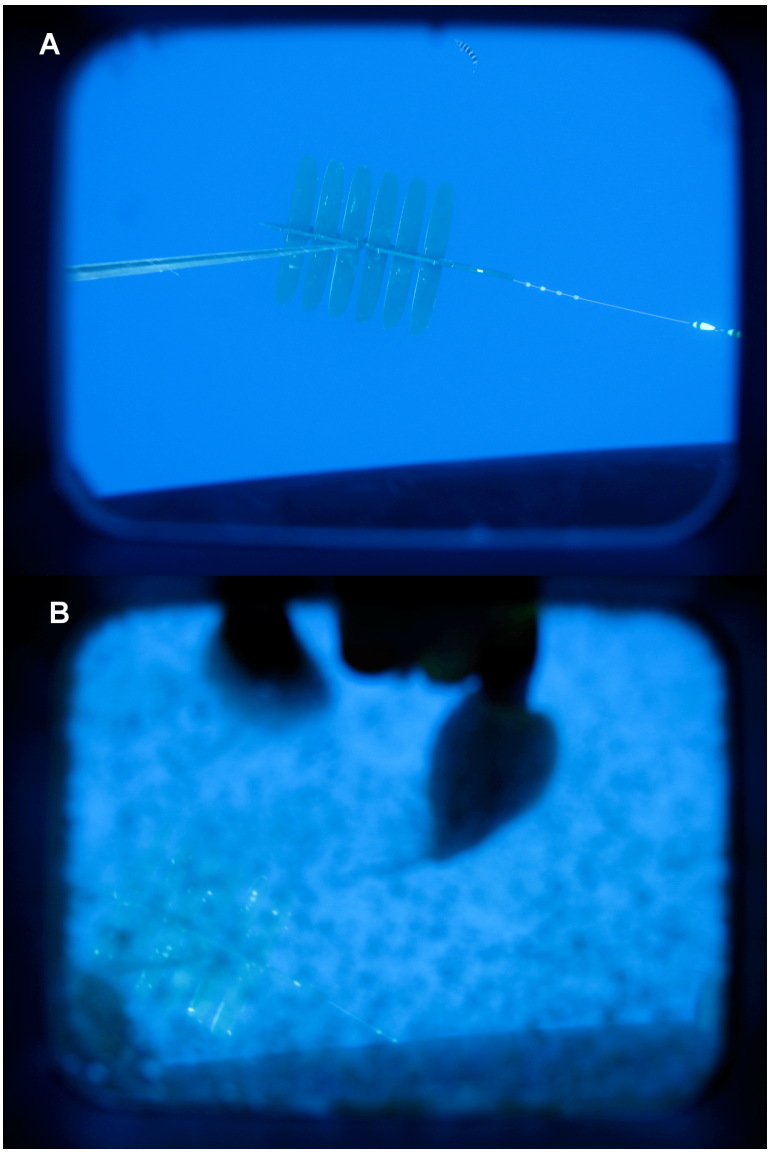

Fig 13. Images from the Downward Facing Camera to compare biofouling. A) No biofouling: 10 July 2015. B) Biofouling: 1 November 2015.

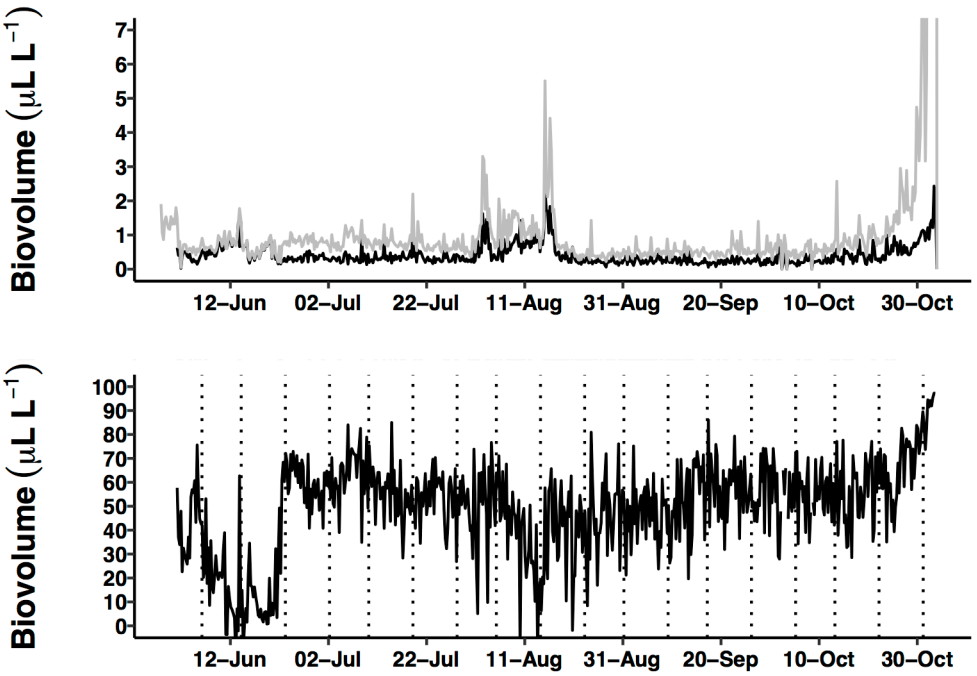

Fig 14. Biovolume calculated from 11-58µm equivalent spherical diameter bins. A) Particle volume calculated from Holo_Batch software. Grey = processing without averaged background removals. Black = processing when averaged holograms are used to remove stationary particles. B) Percentage of biovolume removed from each hologram. Dashed vertical lines show the end of a 510 hologram batch used to calculate biofouling.

The chl data from the Aqua MODIS satellite show weak correlations with the Holo data and F_v:F_m (Fig 6). The correlation between the Aqua MODIS data and both the nighttime average of the F_v:F_m (r^2=0.123) and *Hemiaulus* abundance (r^2=0.091) was poorly correlated. The F_v:F_m data, cell counts, and biovolume peaks correspond to some of the peaks in the satellite detected chl densities. Possible explanations for these weak correlations are discussed in the discussion.

The two Turner C3 fluorometers produced erratic signals and random shifts in baseline values (Fig 15). While, at times, the data appear to be reasonable, the data sets were excluded

from further analysis because it was difficult to tell which data points were reflective of the water properties and which were noise or errors introduced by the sensor.

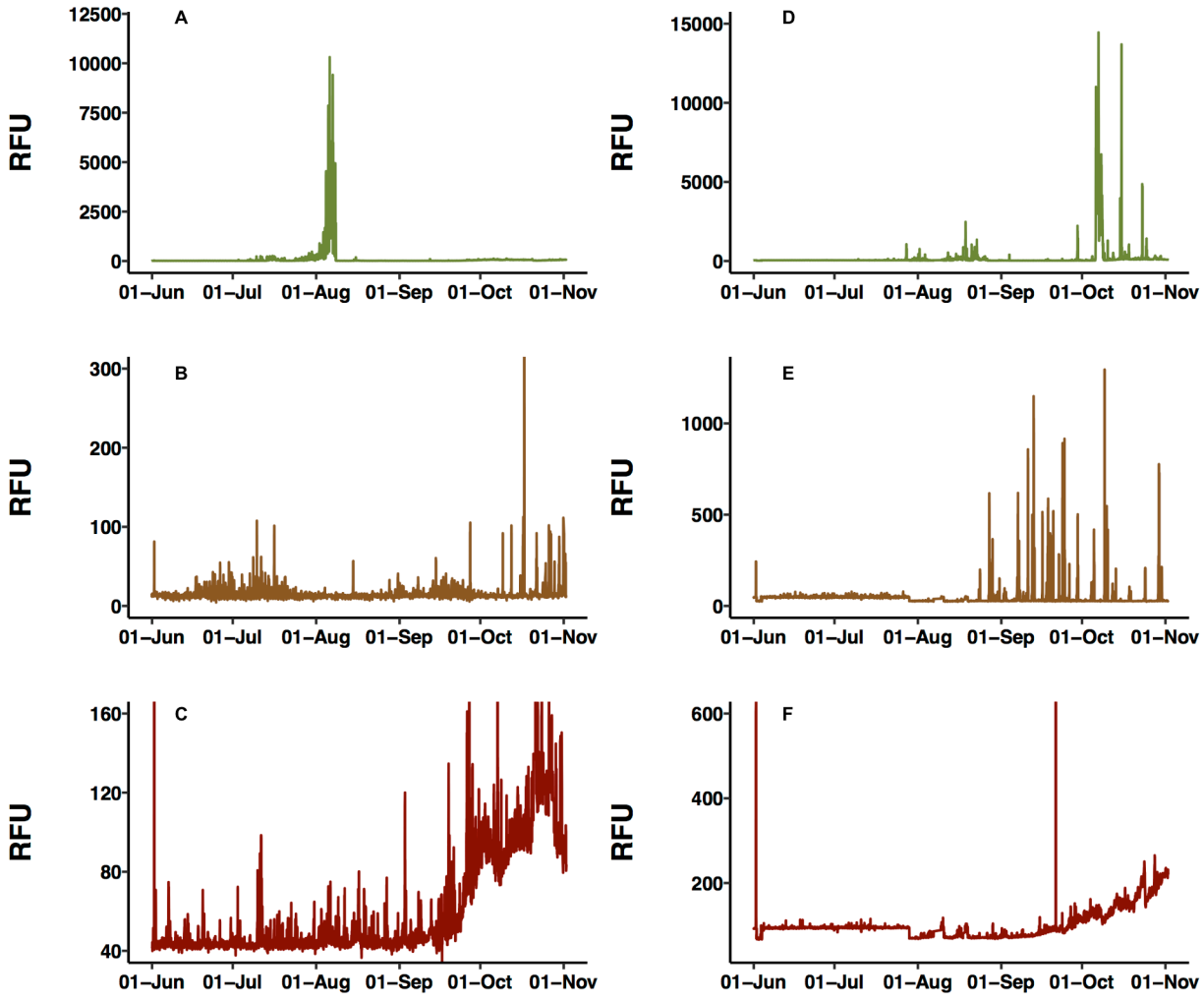

Fig 15. C3 fluorometer data from the *Honey Badger*. Note scale shifts between plots. A-C) Sensor coated with antifouling compound. A) Chl, B) CDOM, C) Phycoerythrin. D-F) uncoated sensor. D) Chl, E) CDOM, F) Phycoerythrin.

Discussion

The Holo data confirm that during the late summer/early timeframe *Hemiaulus* and *Rhizosolenia* diatoms are the dominant diatom genera in the NPSG [24,32] and that *Hemiaulus* aggregates can be found within the region [33]. *Hemiaulus* aggregates occurred throughout the mission, even in regions of low non-aggregated *Hemiaulus* abundance (Fig 9-10). These observations may indicate that aggregated forms of *Hemiaulus* are a natural growth form of *Hemiaulus* and are not a result of high rates of impact between *Hemiaulus* cells as suggested by Jackson's general coagulation model for diatom aggregates [51]. Regularly occurring *Hemiaulus* aggregates could be an important food source to organisms in the open ocean due to their high concentration of carbon and nitrogen. They could also play an important role in the global carbon cycle as aggregated forms tend to sink much faster than non-aggregated particles [52]. They can also act as small nets which take other suspended particles to depth with them [53]. Station ALOHA sediment trap data indicated that during the SEP the sinking of diatoms and diatom aggregates could result in around 20% of the annual carbon export [26]. Trap-collected material captured during the SEP contained a higher number of intact cells, increasing the amount of fixed carbon removed from the air-sea interface. The results of the *Honey Badger* mission indicate that aggregate events appear throughout the NPSG and well outside the SEP (Table 2). The ability of the NPSG to sequester atmospheric carbon in the form of aggregates outside short-term, or geographically isolated, SEPs could indicate that the NPSG plays a much greater role in climate regulation than previously thought.

The biovolume estimates calculated by the Holo_Batch software probably do not accurately represent the volume of the diatoms imaged, but should be provide an acceptable proxy for the relative particle volume of the images. *Rhizosolenia* cells are roughly elongated

cylinders that when viewed in a 3D matrix and allowed to be randomly oriented may be longer than imaged. The conversion of particles into an equivalent spherical diameter may distort the volume of these elongated particles [54]. The estimates for the *Hemiaulus* biovolume is probably closer to the actual cellular volume because the *Hemiaulus* cells are not as elongated and so the dimensions are closer to the sphere-based calculations of the Holo_Batch. Due to these differences the biovolume may not provide an accurate measure of the total particle volume in the sample in $\mu L\ L^{-1}$ but can provide information about the relative particle volume between samples.

Biofouling was a factor which had to be accounted for in our analysis. The Holo contained copper fixtures which would have reduced the algal buildup in the sampling chamber, but the data analysis of the biovolume from the Holo suggests that biofouling still occurred. The Holo_Batch software was useful in filtering out particles which stayed in place through multiple holograms, such as algae or other particles adhered to the optical surfaces. Around 24 June 2015, the percent of biovolume removed during processing increased from an average of 24.6% to an average of 53.8% and remained fairly steady until near the end of the mission. Around 25 October 2015, the percentage removed steadily climbed to 97.3% on 2 November 2015. Although biofouling occurred, it appeared to reach a steady state before entering the waters around the Hawaiian Islands. Prior to 24 June 2015, it appeared that there was a sloughing off event which cleared the optical surfaces, resulting in the decreased average removal percent of 24.6%. Most of the mission was conducted in the oligotrophic waters of the NPSG, as the *Honey Badger* moved into the waters closer to the Hawaiian Islands the biovolume steadily increased to around 2 $\mu L\ L^{-1}$, similar to the values observed in the *Hemiaulus* and *Rhizosolenia* blooms, 1.63

$\mu L\ L^{-1}$ and 2.33 $\mu L\ L^{-1}$. The increase in biovolume and percent of biovolume removed may suggest that the biofouling had become so severe that most of the optical surfaces were covered or that the biofouling had produced filaments which were mobile enough to avoid removal by the averaging Holo_Batch software. In the raw holograms, these later images appear blurry with many very small diffraction patterns which do not come into focus using the Holo_Detail software.

The waypoints for *Honey Badger* were partially chosen based on the Aqua MODIS's chl concentration data. One of the goals of the mission was to sample regions with a chl concentration >0.15 mg m^{-3} so the satellite data was used to try to find and intercept these regions. The 8-day composite of the Aqua MODIS satellite data provides a more complete image of the regional chl concentrations, as daily images often are incomplete due to cloud cover. However, this means that the images used for daily decision making on the glider's movements were based on data that was 4 days old. This delay could have resulted in a few missed sampling opportunities (https://youtu.be/xYE39ua_NTc) because by the time we were able to look at chl maps of the region the data was already outdated by a few days.

We found no evidence of iron limitation. Nitrogen fixation requires a ready supply of iron and phosphorous [45,55] yet during the *Hemiaulus* and *Rhizosolenia* blooms observed on 3 August 2015 and 16 August 2015 the PhytoFlash did not indicate that they were experiencing iron limitation or iron stress. Although the PhytoFlash had to be rebooted frequently and failed in early September, the diel F_v:F_m patterns helped characterize the nutrient limitation trends of the region when it was operational. The lack of evidence for iron limitation in the region suggests that sufficient iron is being supplied from some outside source (upwelling or atmospheric

deposition) [38,56], that the diazotrophic cells were limited by a different nutrient [3,4,6,57], or that diazotrophic cells were being limited by competition with non-diazotrophic cells [5]. From 1 June 2015 to 31 October 2015, the dark-averaged F_v:F_m stayed above the light-averaged values, agreeing with the 2006 study by Behrenfeld et al. [58] which classified this area as having a type I regime with low macronutrients but sufficient iron supplies.

Conclusion

The *Honey Badger* offered a unique look into the remote oligotrophic North Pacific subtropical gyre during its 5690 km mission. While it was a disappointment that some of the sensors failed during the mission (PhytoFlash), or started producing uninterpretable data (C3s), the mission was a success in that other sensors (Holo) recorded novel data over an extensive period of time (5-months) and wide geographic extent. *The Honey Badger* and its sensors allowed for a persistent presence in the NPSG during the late summer/early fall bloom season.

The PhytoFlash data indicated that the region did not experience iron limitation despite the presence of DDAs. *Hemiaulus* aggregates were observed outside the 15 July – 15 August SEP [26] window suggesting the carbon sequestering capabilities of the NPSG is greater than previously thought if aggregates are consistent vectors for transport. Conversely, the widespread distribution and lack of relationship with *Hemiaulus* abundance may indicate they are a growth form of *Hemiaulus* similar to *Rhizosolenia* mats [59]. The PhytoFlash and the Holo data are generally uncorrelated with satellite chl concentrations which illustrates the necessity of *in situ* sampling to understand the community structure and physiology occurring within remote open ocean habitats.

References

1. Guieu C, Aumont O, Paytan A, Bopp L, Law CS, Mahowald N, et al. The significance of the episodic nature of atmospheric deposition to Low Nutrient Low Chlorophyll regions. Global Biogeochem Cycles. 2014;28:1179–1198.
2. Carpenter EJ, Capone DG. Nitrogen fixation in the marine environment. In: Capone DG, Bronk DA, Mulholland MR, Carpenter EJ, editors. Nitrogen in the Marine Environment. Elsevier; 2008. p. 141–198.
3. Mills M, Ridame C, Davey M, La Roche J, Geider R. Iron and phosphorus co-limit nitrogen fixation in the eastern tropical North Atlantic. Nature. 2004;429(6989):292–4.
4. Ratten J, LaRoche J, Desai DK, Shelley RU, Landing WM, Boyle E, et al. Sources of iron and phosphate affect the distribution of diazotrophs in the North Atlantic. Deep-Sea Res Part II-Top Stud Oceanogr. 2015;116:332–341.
5. Weber T, Deutsch C. Local versus basin-scale limitation of marine nitrogen fixation. Proc Natl Acad Sci U S A. 2014;111(24):8741–8746.
6. Kustka A, Carpenter EJ, Sañudo-Wilhelmy SA. Iron and marine nitrogen fixation: progress and future directions. Res Microbiol. 2002;153:255–262.
7. Zehr JP, Kudela RM. Nitrogen cycle of the open ocean: From genes to ecosystems. Ann Rev Mar Sci. 2011;3:197–225.
8. Goering JJ, Dugdale RC, Menzel DW. Estimates of *in situ* rates of nitrogen uptake by *Trichodesmium* sp. in the tropical Atlantic Ocean. Limnol Oceanogr. 1966;11(4):614–20.
9. Capone DG, Zehr JP, Paerl HW, Bergman B, Carpenter EJ. *Trichodesmium*, a globally significant marine cyanobacterium. Science. 1997;276(5316):1221–1229.

10. Zehr JP, Waterbury JB, Turner PJ, Montoya JP, Omoregie E, Steward G, et al. Unicellular cyanobacteria fix N_2 in the subtropical North Pacific Ocean. Nature. 2001;412:635–638.

11. Goebel NL, Edwards CA, Carter BJ, Achilles KM, Zehr JP. Growth and carbon content of three different-sized diazotrophic cyanobacteria observed in the subtropical North Pacific. J Phycol. 2008;44:1212–1220.

12. Thompson A, Carter BJ, Turk-Kubo K, Malfatti F, Azam F, Zehr JP. Genetic diversity of the unicellular nitrogen-fixing cyanobacteria UCYN-A and its prymnesiophyte host. Environ Microbiol. 2014;16(10):3238–3249.

13. Thompson AW, Foster RA, Krupke A, Carter BJ, Musat N, Vaulot D, et al. Unicellular cyanobacterium symbiotic with a single-celled eukaryotic alga. Science. 2012;337:1546–1550.

14. Foster RA, Carpenter EJ, Bergman B. Unicellular cyanobionts in open ocean dinoflagellates, radiolarians, and tintinnids: Ultrastructural characterization and immuno-localization of phycoerythrin and nitrogenase. J Phycol. 2006;42:453–463.

15. Farnelid H, Tarangkoon W, Hansen G, Hansen PJ, Riemann L. Putative N_2-fixing heterotrophic bacteria associated with dinoflagellate–*Cyanobacteria* consortia in the low-nitrogen Indian Ocean. Aquat Microb Ecol. 2010;61:105–117.

16. Villareal T. Marine nitrogen-fixing diatom-cyanobacterial symbioses. In: Carpenterl EJ, Capone DG, Reuter J, editors. Marine Pelagic Cyanobacteria: *Trichodesmium* and other Diazotrophs. Netherlands: Kluwer; 1992. p. 163–175.

17. Foster RA, O'Mullan GD. Nitrogen-fixing and nitrifying symbioses in the marine environment. In: Capone DG, Bronk D, Mulholland MR, Carpenter EJ, editors. Nitrogen in the Marine Environment. 2nd ed. San Diego, CA: Elsevier; 2008. p. 1197–1218.

18. Hilton JA, Foster RA, Tripp HJ, Carter BJ, Zehr JP, Villareal TA. Genomic deletions disrupt nitrogen metabolism pathways of a cyanobacterial diatom symbiont. Nat Commun. 2013;4:1767.

19. Foster R, Zehr JP. Characterization of diatom-cyanobacteria symbioses on the basis of nifH, hetR and 16S rRNA sequences. Environ Microbiol. 2006;8:1913–1925.

20. Carpenterl EJ, Montoya JP, Burns J, Mulholland MR, Subramaniam A, Capone DG. Extensive bloom of a N_2-fixing diatom/cyanobacterial association in the tropical Atlantic Ocean. Mar Ecol Prog Ser. 1999;185:273–283.

21. Subramaniam A, Yager PL, Carpenter EJ, Mahaffey C, Björkman KM, Cooley S, et al. Amazon River enhances diazotrophy and carbon sequestration in the tropical North Atlantic Ocean. Proc Natl Acad Sci U S A. 2008;105(30):10460–10465.

22. Bombar D, Moisander PH, Dippner JW, Foster RA, Vos M, Karfeld B, et al. Distribution of diazotrophic microorganisms and nifH gene expression in the Mekong River plume during intermonsoon. Mar Ecol Prog Ser. 2011;424:39–52.

23. Church MJ, Björkman KM, Karl DM, Saito MA, Zehr JP. Regional distributions of nitrogen-fixing bacteria in the Pacific Ocean. Limnol Oceanogr. 2008;53(1):63–77.

24. Scharek R, Tupas LM, Karl DM. Diatom fluxes to the deep sea in the oligotrophic North Pacific gyre at Station ALOHA. Mar Ecol Prog Ser. 1999;182:55–67.

25. Scharek R, Latasa M, Karl DM, Bidigare RR. Temporal variations in diatom abundance and downward vertical flux in the oligotrophic North Pacific gyre. Deep Res I. 1999;46:1051–1075.

26. Karl DM, Church MJ, Dore JE, Letelier RM, Mahaffey C. Predictable and efficient carbon sequestration in the North Pacific Ocean supported by symbiotic nitrogen fixation. PNAS.

2012;109(6):1842–1849.

27. White AE, Spitz YH, Letelier RM. What factors are driving summer phytoplankton blooms in the North Pacific Subtropical Gyre? J Geophys Res. 2007;112:C12006.

28. Dore JE, Letelier RM, Church MJ, Lukas R, Karl DM. Summer phytoplankton blooms in the oligotrophic North Pacific Subtropical Gyre: Historical perspective and recent observations. Progress in Oceanography. 2008;76:2–38.

29. Fong AA, Karl DM, Lukas R, Letelier RM, Zehr JP, Church MJ. Nitrogen fixation in an anticyclonic eddy in the oligotrophic North Pacific Ocean. ISME J. 2008;2:663–676.

30. Venrick EL. The vertical distributions of chlorophyll and phytoplankton species in the North Pacific central environment. J Plankton Res. 1988;10:987–998.

31. Venrick EL. Phytoplankton species structure in the central North Pacific, 1973–1996: variability and persistence. J Plankton Res. 1999;21(6):1029–1042.

32. Venrick EL. The distribution and significance of *Richelia intracellularis* Schmidt in the North Pacific Central Gyre. Limnol Oceanogr. 1974;19(3):437–445.

33. Villareal TA, Brown CG, Brzezinski MA, Krause JW, Wilson C. Summer diatom blooms in the North Pacific Subtropical Gyre: 2008–2009. PLoS One. 2012;7(4):e33109.

34. Villareal TA, Adornato L, Wilson C, Schoenbaechler CA. Summer blooms of diatom-diazotroph assemblages and surface chlorophyll in the North Pacific gyre: A disconnect. J Geophys Res. 2011;116:C03001.

35. Brzezinski MA, Villareal TA, Lipschultz F. Silica production and the contribution of diatoms to new and primary production in the central North Pacific. Mar Ecol Prog Ser. 1998;167:89–104.

36. Wilson C, Qiu X. Global distribution of summer chlorophyll blooms in the oligotrophic

gyres. Prog Oceanogr. 2008;78(2):107–34.

37. Wilson C. Late summer chlorophyll blooms in the oligotrophic North Pacific Subtropical Gyre. Geophys Res Lett. 2003;30(18):1942.

38. Dore JE, Brum JR, Tupas LM, Karl DM. Seasonal and interannual variability in sources of nitrogen supporting export in the oligotrophic subtropical North Pacific Ocean. Limnol Oceanogr. 2002;47(6):1595–1607.

39. Daniel T, Manley J, Trenaman N. The Wave Glider: enabling a new approach to persistent ocean observation and research. Ocean Dyn. 2011;61:1509–1520.

40. Villareal TA, Wilson C. A Comparison of the Pac-X Trans-Pacific wave glider data and satellite data (MODIS, Aquarius, TRMM and VIIRS). PLoS One. 2014;9(3):e92280.

41. Hine R, Willcox S, Hine G, Richardson T. The wave glider: A wave-powered autonomous marine vehicle. Proc of MTS/IEEE OCEANS. 2009.

42. Liquid Robotics Inc. Flexible Design Supports Wide Range of Sensors and Payloads. 2017 [cited 2017 Dec 6]. Available from: https://www.liquid-robotics.com/platform/supported-sensors/

43. Davies EJ, Buscombe D, Graham GW, Nimmo-Smith WAM. Evaluating unsupervised methods to size and classify suspended particles using digital in-line holography. J Atmos Ocean Technol. 2015;32(6):1241–1256.

44. Andrews SW, Nover DM, Reuter JE, Schladow SG. Limitations of laser diffraction for measuring fine particles in oligotrophic systems: Pitfalls and potential solutions. Water Resour Res. 2011;47:W05523.

45. Behrenfeld MJ, Milligan AJ. Photophysiological expressions of iron stress in phytoplankton. Ann Rev Mar Sci. 2013;5:217–246.

46. ESRI 2011. ArcGIS Desktop. Redlands, CA: Environmental Systems Research Institute;

47. RStudio Team. RStudio: Integrated Development for R. [Internet]. Boston, MA: RStudio, Inc.; 2016. Available from: http://www.rstudio.com/

48. Wilson C, Villareal TA, Brzezinski MA, Krause JW, Shcherbina AY. Chlorophyll bloom development and the subtropical front in the North Pacific. J Geophys Res Ocean. 2013;118(3):1473–1488.

49. Rasband WS. ImageJ. Bethesda, MA: National Institutes of Health; Available from: https://imagej.nih.gov/ij/

50. Behrenfeld MJ, Kolber ZS. Widespread iron limitation of phytoplankton in the South Pacific Ocean. Science. 1999;283:840–843.

51. Jackson GA. A model for the formation of marine algal flocs by physical coagulation processes. Deep Res. 1990;37(8):1197–1211.

52. Stemmann L, Boss E. Plankton and particle size and packaging: From determining optical properties to driving the biological pump. Ann Rev Mar Sci. 2012;4(1):263–290.

53. Alldredge AL, Silver MW. Characteristics, dynamics and significance of marine snow. Prog Oceanogr. 1988;20:41–82.

54. Mustard AT, Anderson TR. Use of spherical and spheroidal models to calculate zooplankton biovolume from particle equivalent spherical diameter as measured by an optical plankton counter. Limnol Oceanogr Methods. 2005;3:183–189.

55. Karl D, Michaels A, Bergman B, Capone D, Carpenter E, Letelier R, et al. Dinitrogen fixation in the world's oceans. Biogeochemistry. 2002;57/58:47–98.

56. Calil PHR, Richards KJ. Transient upwelling hot spots in the oligotrophic North Pacific. J Geophys Res. 2010;115:C02003.

57. Moore JK, Doney SC. Iron availability limits the ocean nitrogen inventory stabilizing feedbacks between marine denitrification and nitrogen fixation. Global Biogeochem Cycles. 2007;21:GB2001.

58. Behrenfeld MJ, Worthington K, Sherrell RM, Chavez FP, Strutton P, Mcphaden M, et al. Controls on tropical Pacific Ocean productivity revealed through nutrient stress diagnostics. Nature. 2006;442:1025–1028.

59. Villareal TA, Pilskaln CH, Montoya JP, Dennett M. Upward nitrate transport by phytoplankton in oceanic waters: balancing nutrient budgets in oligotrophic seas. PeerJ. 2014;2:e203.

Vita

Emily Elizabeth Anderson was born in Columbia, MO in 1989. She attended Columbia Independent School from 6-12 grade and then moved on to attend the University of Missouri in 2008 where she earned her Bachelor of Science in Biology in 2012. She worked at the Boone County Health Department and the University of Missouri Health Management and Informatics department until she began her work towards a Master's Degree with the University of Texas at Austin's Marine Science Institute in 2015. While working towards her Master's Degree in Port Aransas, TX she volunteered at the Animal Rehabilitation Keep (renamed the Amos Rehabilitation Keep) or ARK, where she worked with injured coastal birds and wildlife. After Hurricane Harvey destroyed Port Aransas she relocated with other classmates to continue her studies in Corpus Christi, TX and the University of Texas A & M – Corpus Christi.

Address: andersonee89@gmail.com

This manuscript was typed by the author.